IIETA International Information and Engineering Technology Association
Advancing the World of Information and Engineering

Annales de Chimie - Science des Matériaux
Vol. 50, No. 3, June, 2026, pp. 293-302
Journal homepage: http://iieta.org/journals/acsm

Electrochemical Synthesis of PHO-SiO_2/Al_2O_3 Nanocomposite Coatings for Corrosion Protection of Low-Carbon Steel Alloy

Ayat Monther Alqudsi[1], Zainab Hussain[2], Ali Hussein Ghanim[3], Yaman Khalid Sadeq[4], Omar A. Alwash[1*]

[1] Scientific Research Commission, Baghdad 10070, Iraq
[2] Department of Chemistry, College of Science, Misan University, Misan 62001, Iraq
[3] Department of Chemistry, College of Science, Baghdad University, Baghdad 10071, Iraq
[4] Department of Forensic Evidence, College of Science, Al-Farahidi University, Baghdad 10011, Iraq

Corresponding Author Email: omar.a.alwash@src.edu.iq

https://doi.org/10.18280/acsm.500309

Received: 11 April 2026
Revised: 12 June 2026
Accepted: 19 June 2026
Available online: 30 June 2026

Keywords:
conducting polymer, corrosion, electropolymerization, low-carbon steel, nanocomposite, Tafel analysis

ABSTRACT

Electropolymerized poly[(Z)-4-((4-hydroxyphenyl) amino)-4-oxobut-2-enoic acid] (PHO) nanocomposite films containing SiO_2 and Al_2O_3 nanoparticles were prepared on low-carbon steel (LCS) to improve protection against corrosion in 3.5 wt.% NaCl. The coatings were deposited under optimized electropolymerization conditions to obtain uniform and adherent barrier layers. The corrosion behavior of bare steel, neat PHO, and nanoparticle-modified PHO coatings was assessed at 298-318 K using potentiodynamic polarization and electrochemical impedance spectroscopy (EIS). All coated samples showed a significant reduction in corrosion current density (I_{corr}) and a marked increase in corrosion resistance compared with uncoated LCS. Incorporation of metal oxide nanoparticles enhanced the compactness and protective ability of the polymer matrix. Among the tested systems, PHO/SiO_2 provided the highest Polarization Resistance (R_p), whereas PHO/Al_2O_3 offered superior protection efficiency and thermal stability at higher temperatures. AFM observations confirmed dense, homogeneous surfaces with smaller grain size after nanoparticle addition. Kinetic and thermodynamic analyses indicated improved Rp and modified activation parameters, suggesting that PHO-based nanocomposite coatings are promising protective layers for LCS exposed to saline environments.

1. INTRODUCTION

Low carbon steel (LCS) corrosion has become one of the most important industrial problems, thanks to its application in the petroleum, marine, and chemical industries. The electrochemical deterioration of LCS surfaces is expedited through aggressive environments with chloride ion-heavy environmental conditions, resulting in serious economic and environmental problems due to the rapid electrochemical loss of the steel surface with corrosion. As a result, developing efficient, protective coatings with high corrosion resistance to the environment is one of the most relevant areas of research [1].

Conductive polymers prepared with electrochemical polymerization have attracted a great deal of attention because they possess good adhesion, electrochemical activity, and anti-corrosion effect [2]. Moreover, conductive polymers can serve as selective protective barriers that reduce the penetration of corrosive species onto metallic surfaces and make them more durable in hostile environments [3]. Polymeric coatings are widely applied in preventing corrosion due to their convenience in preparation and their good chemical, thermal, and mechanical properties [4].

Conventional polymeric coatings have shortcomings, however. For instance, poorly-packed microstructures and coating defects are present, allowing corrosive ions to penetrate more easily and reducing the lasting benefits of the process [5]. Recent studies have thus shifted towards integrating nanoparticles into polymer matrices to enhance coating compactness, barrier properties, and corrosion resistance. Polymer-based nanocomposites are promising because of synergistic interactions between polymer matrices and nanomaterials [6].

Mathai and Shaji [6] reviewed polymer-based nanocomposite coating approaches and found that nanocomposite coatings showed superior barrier performance, corrosion resistance, and mechanical stability when compared to conventional polymer coatings.

However, they also reported that the long-term coating stability under extreme conditions remains a great challenge. Alqudsi and Saleh [7] applied electrochemical polymerization to eugenol and evaluated the corrosion protection of stainless steel 304 L. They also proved that electropolymerized coatings could effectively lower corrosion current density (I_{corr}) as well as promote corrosion resistance in harsh media.

Huang et al. [8] prepared electroactive epoxy-SiO_2 hybrid nanocomposite coatings and found that SiO_2 nanoparticles increased coating compactness and enhanced anticorrosive

behavior through decreased diffusion pathways of corrosive species.

Yeganeh and Keyvani [9] studied mesoporous silica nanocontainment as part of a polymer coating, where silica nanoparticles are found to have a corrosion resistance effect by limiting the corrosive mediums from penetrating to the defective and damaged coating regions. Wang et al. [10] studied epoxy/alumina nanocomposites, and the addition of Al_2O_3 nanoparticles resulted in increased morphology and mechanical stability of the polymer matrix and enhanced coating performance.

Balaraju et al. [11] studied Ni-P-Al_2O_3 composite coatings and found that alumina nanoparticles substantially increased the hardness, compactness, and corrosion resistance of the coating because of improved microstructures. Tallman et al. [12] established a novel approach for corrosion protection in developing nano-composite coatings with polypyrrole and alumina nanoparticles.

The results showed that the stability and protective performance of polymer conductive coatings under corrosive environments [12] was improved by Al_2O_3 nanoparticles.

Previous results showed the excellent enhancement during the process of electropolymerizing poly[(Z)-4-((4-hydroxyphenyl) amino)-4-oxobut-2-enoic acid] (PHO) on LCS surfaces. In fact, although there has been considerable improvement in the performance of conductive polymer nanocomposite coatings, little work on such coatings has been conducted on the electropolymerization of PHO.

Moreover, not enough work has been conducted on the comparative effects of SiO_2 and Al_2O_3 nanoparticles on the electrochemical properties, thermal stability, and surface morphology of PHO coatings at different temperatures. Thus, in this work, we intend to explore the synthesis of PHO- and PHO-based nanocomposite coatings on LCS surfaces by means of electropolymerization and assess their corrosion protection potentials against 3.5 wt.% NaCl solution with varying temperature options.

2. MATERIALS AND METHODS

2.1 Metal preparation

LCS plates with a thickness of 15 mm and dimensions of 2 × 2 cm^2 were employed as substrate materials in this study. Prior to coating, the samples were mechanically cut into circular discs with a diameter of 25 mm. Surface pretreatment was carried out by successive grinding with silicon carbide abrasive papers of different grit sizes, namely 180, 220, 400, 1200, 2000, and 2500 mesh. The polished specimens were then rinsed thoroughly with distilled water followed by tap water, degreased using acetone, and subsequently cleaned with absolute ethanol. Finally, the samples were dried with hot air using a heat gun and kept in a desiccator overnight before further use [13].

2.2 Electrochemical process

Using 0.1 M (Z)-4-((4-hydroxyphenyl) amino)-4-oxobut-2-enoic acid (HO) as the monomer and 0.1 g of both Silicon dioxide (SiO_2) and Aluminum oxide (Al_2O_3) added to 100 mL distilled water with three drops of H_2SO_4, polymerization was performed electrochemically on LCS electrodes with a graphene counter electrode at 2 V with a DC-power supply for 60 min at room temperature. The electropolymer formation process was followed by cyclic voltammetry (scan rate of 20 mV/s) on the Pt electrode. Polymerization was achieved over a range of -0.20 to 1.5 V. The overall electropolymerization equation of the HO monomer to form the PHO polymer is illustrated in Figure 1.

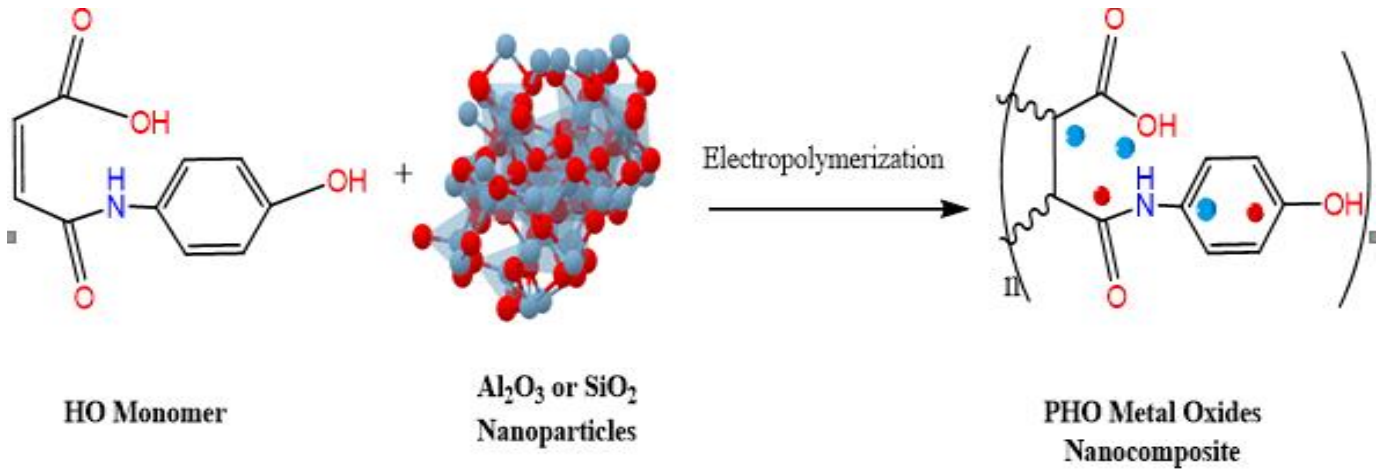

Figure 1. General equation of electropolymerization of (Z)-4-((4-hydroxyphenyl) amino)-4-oxobut-2-enoic acid (HO) monomer

2.3 Corrosion studies

Using Tafel extrapolation method, and an aqueous solution of 3.5 wt.% NaCl, the efficiency of corrosion inhibitors was evaluated at temperature range 298-318 K. This method was tested using a standard 3-electrode cell assembly (WENKING M Lab-200 Bank Electronik-Intelligent controls GmbH), where LCS served as the working electrode, platinum served as the counter electrode, and each test contained a saturated calomel electrode (SCE) as the reference electrode [14].

3. RESULTS AND DISCUSSION

3.1 Cyclic voltammetry and electro-polymerization of the (Z)-4-((4-hydroxyphenyl) amino)-4-oxobut-2-enoic acid monomer

The electrochemical growth behavior of 0.1 gm HO monomer in 3.5% NaCl solution. Because the solution exhibited low conductivity, three drops of concentrated H_2SO_4 were added to improve conductivity, as shown in Figure 2. The

evolution of the electropolymerization process was performed by cyclic voltammetry via sweeping potential in the range: −2000 to +2000 mV vs. SCE at a scan rate of 550 mV/s.

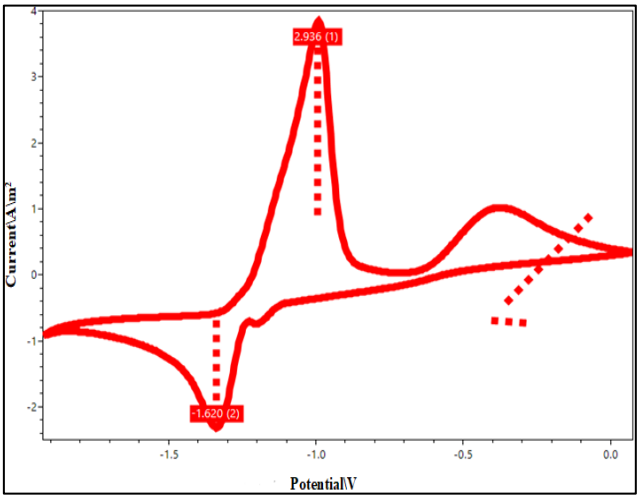

Figure 2. The cyclic voltammogram of HO
Note: HO = (Z)-4-((4-hydroxyphenyl) amino)-4-oxobut-2-enoic acid

The cyclic voltammogram of HO exhibits an anodic peak at approximately 2.936 V during the forward scan, which may be associated with the oxidation of the HO monomer. During the reverse scan, a cathodic peak appears, indicating the reduction of electroactive species formed during the anodic process. The observed changes in the voltammetric response after successive scans suggest the possible formation of a surface layer on the electrode. These results are consistent with previous reports describing the electrochemical oxidation behavior of HO and the potential formation of polymeric films on electrode surfaces. However, additional surface and structural characterization techniques are required to conclusively confirm electropolymerization and film deposition mechanisms [15], as shown in Figure 2.

3.2 Proposed polymerization mechanism of (Z)-4-((4-hydroxyphenyl) amino)-4-oxobut-2-enoic acid on low-carbon steel electrode

The electropolymerization of the HO monomer on the LCS electrode surface to form the PHO polymer coating was performed through cationic polymerization, which is carried out in the following phases [16].

(1) When anodic potential is applied to monomer solutions, electrons are extracted from monomers to electrodes, forming cationic radicals on the electrode surface (Steps 1-2 of Figure 3). The functional groups of monomers and Fe atoms (from LCS) interact to facilitate adsorption between monomers and electrodes; therefore, there is a lack of electrons on the electrode surface, resulting in the physical interaction of cationic radicals to form cationic radicals on lead electrodes.

(2) To form larger molecules, the cationic radicals formed react with nearby monomers that are uncharged. This is accomplished via a cationic addition mechanism at the oxidized monomers' charged end (refer to steps 3 through 4 in the figure provided).

(3) During the coupling process shown in Steps 3 to 4, protons (H^+) are released from the monomer units. This step is crucial for the formation of stable covalent bonds between the units, allowing the polymer chain to grow effectively on the surface. This process continues with the addition of more monomer units to the growing chain. Anions from the electrolyte solution stabilize the cationic centers, ensuring the continuous buildup of the polymeric structure across the LCS electrode surface.

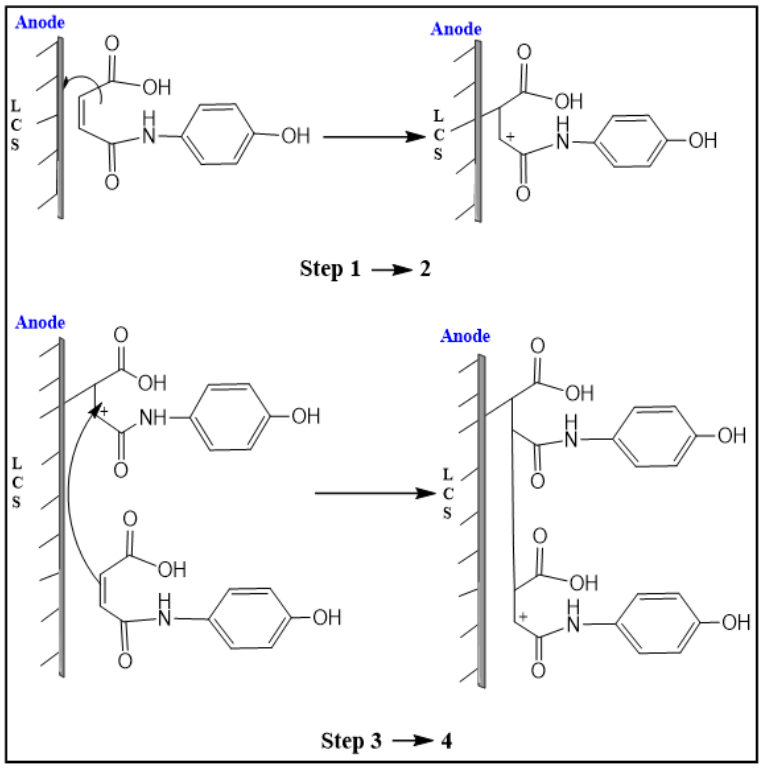

Figure 3. Proposed electropolymerization mechanism of HO at the LCS electrode
Note: HO = (Z)-4-((4-hydroxyphenyl) amino)-4-oxobut-2-enoic acid.

3.3 Fourier transform infrared spectroscopy characterization of (Z)-4-((4-hydroxyphenyl) amino)-4-oxobut-2-enoic acid electropolymerization to form poly[(Z)-4-((4-hydroxyphenyl) amino)-4-oxobut-2-enoic acid]

The Fourier transform infrared spectroscopy (FTIR) spectra of the HO monomer and the PHO polymer, as seen in Figure 4, give insight into the functional groups found in the polymer and its overall structure as applied onto the LCS electrode. The FTIR spectrum for the monomer (Figure 4(A)) shows that there are bands attributed to carboxylic O–H, N–H, and C–H stretching at 2983.67 cm^{-1}, and that the C = O bands for C = O carboxylic acid and C =O amide were just overlapped/appeared in the same region at 1699.17 cm -1; and that there was a broad band at 1573.81 due to a C = C ring. The disappearance of the olefinic C=C bands in Figure 4(B) indicates the formation of the PHO polymer. Due to the form of international chains covering the new area of dispersion for polymer PHO, a very wide transmission peak was created [17].

3.4 Analysis of Atomic Force Microscopy

Utilizing atomic force microscopy (AFM), the surface morphology of LCS discs with and without the polymer coating is assessed through an examination under the microscope. 3D images of the polymer and polymer nanocomposites created in the presence and absence of nanoparticles can be seen in Figure 5, respectively. The average roughness (Sa), root mean square roughness (Sq), and primary grain size values obtained from this study are shown in Table 1 and can be used to quantitatively describe the surface characteristics of the materials being researched.

The results indicate that the incorporation of nano metal oxides significantly influenced the surface morphology and grain distribution. For the PHO/Al_2O_3 nanocomposite, a noticeable decrease in surface roughness was observed (Sa = 28.11 nm) compared to the pure PHO film (Sa = 31.97 nm). This improvement in surface smoothness is attributed to the reduction in the main grain size from 161.2 nm to 89.91 nm, suggesting that Al_2O_3 nanoparticles effectively filled the polymer matrix voids and promoted a more compact arrangement. On the other hand, the PHO/SiO_2 nanocomposite exhibited a different trend, where the surface roughness increased to Sa = 50.32 nm. Despite the reduction in grain size to 94.87 nm, the higher Sa and Sq values suggest the formation of a more complex surface texture or slight nanoparticle aggregation.

In conclusion, the significant reduction in grain size observed for both nanocomposites confirms a high degree of integration within the polymer chains. This modification in surface topography is expected to enhance the barrier properties of the coating, where the more compact and refined grain structure provides a denser protective layer against corrosive environments [18].

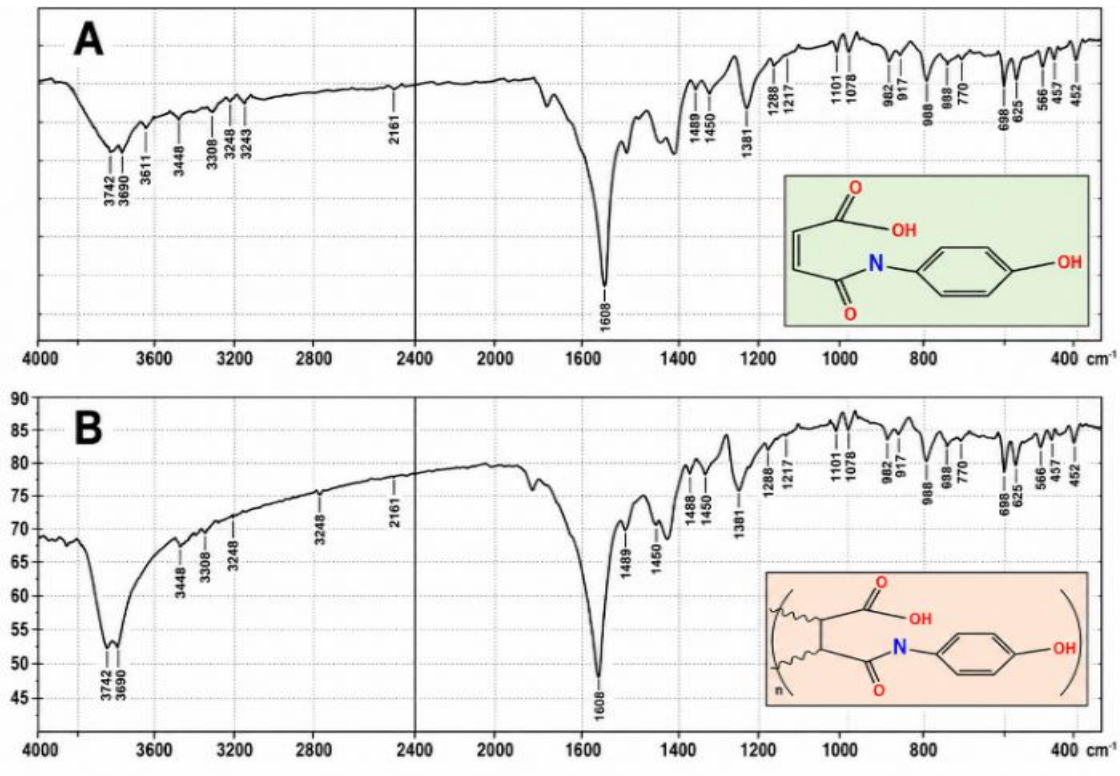

Figure 4. Presents FTIR spectra (A) HO and (B) PHO polymer
Note: HO = (Z)-4-((4-hydroxyphenyl) amino)-4-oxobut-2-enoic acid; PHO = poly[(Z)-4-((4-hydroxyphenyl) amino)-4-oxobut-2-enoic acid].

Table 1. The parameters of AFM of PHO-coated LCS with and without nanoparticles

System	Sa(nm)	Sq(nm)	Main Grain Size(nm)
PHO	31.97	43.95	161.2
PHO\Al_2O_3 nanocomposite	28.11	38.31	89.91
PHO\SiO_2 nanocomposite	50.32	72.45	94.87

Note: AFM = atomic force microscopy; PHO = poly[(Z)-4-((4-hydroxyphenyl) amino)-4-oxobut-2-enoic acid]; LCS = low carbon steel.

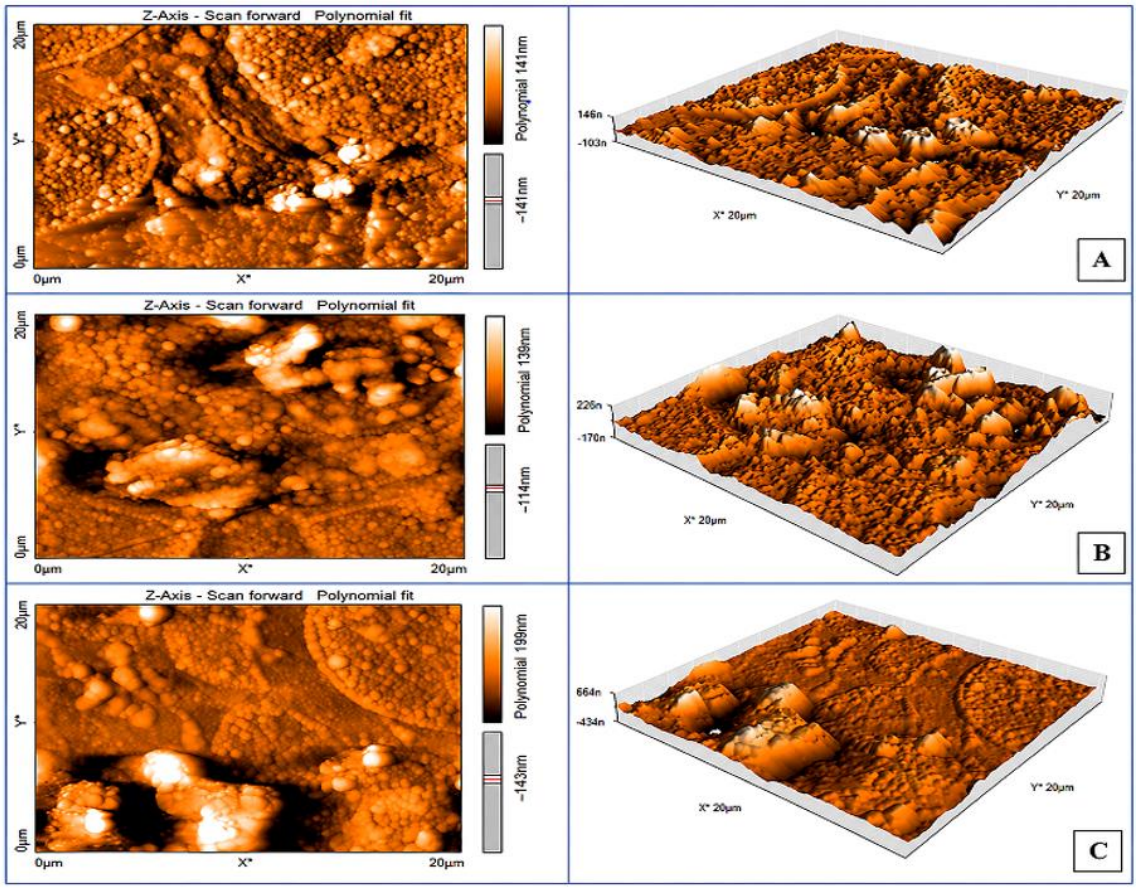

Figure 5. Two and three-dimensional AFM images of (A) PHO-coated LCS, (B) PHO-coated Al_2O_3 nanocomposite, and (C) PHO-coated SiO_2 nanocomposite

Note: AFM = atomic force microscopy; PHO = poly[(Z)-4-((4-hydroxyphenyl) amino)-4-oxobut-2-enoic acid].

3.5 Corrosion studies

Typical polarization curves for coated and uncoated LCS with produced polymer before and after utilizing nanomaterial in a 3.5% sodium chloride (NaCl) solution with a temperature range of (298-318) K are shown in Figure 6. The protective efficacy is calculated using the following Eq. (1) [19].

$$PE\% = \frac{i_{corr,uncoated} - i_{corr,coated}}{i_{corr,uncoated}} \times 100 \qquad (1)$$

The current density of the corrosion current (I_{corr}) in coated and uncoated LCS, i.e., (I_{corr}) unc. and (I_{corr}) c., respectively, is determined as the extrapolation of the corrosion potential (E_{corr}) of the anodic and cathodic Tafel lines. The polarization resistance (R_p) can be computed using the rearranged Stern-Geary equation [20].

$$R_p = \frac{B_a|B_c|}{2.303(B_a + |B_c|)i_{corr}} \qquad (2)$$

The protective performance of electrodeposited coatings is evaluated using R_p measurements, as R_p values are inversely proportional to the i_{corr}. Consequently, a higher R_p indicates a lower corrosion rate and enhanced coating durability. R_p represents the material's kinetic resistance to anodic oxidation under an applied external voltage, providing a quantitative measure of the specimen's ability to withstand degradation in polarized environments.

The electrochemical properties of uncoated LCS and samples coated with PHO and its nanocomposites (Al_2O_3 and SiO_2) at three different temperatures (298, 308, and 318 K) are shown in Table 2. The uncoated alloy had a much worse corrosion resistance than the uncoated LCS (LCS/PHO), but adding nano-fillers (SiO_2 and Al_2O_3) improved the LCS/PHO's protective performance significantly. The corrosion resistance (Rp) data at 298 K confirms the lowest Rp value (145.5 Ω/cm²) of the uncoated LCS alloy, indicating a very high corrosion rate in the saline region. The Rp significantly increased to 2142 Ω/cm² when coating the alloy with just polymer (LCS/PHO). The increase can be ascribed to the development of a barrier layer preventing the passage of ions and corrosive particles to the metal surface. It was revealed that the corrosion resistance was enhanced further by the addition of nano-oxides into the polymer coating. The Rp value obtained was 2563 Ω/cm² when aluminum nano-oxide (Al_2O_3) was added, and the highest value, measured to be 3517 Ω/cm², was recorded when silicon nano-oxide (SiO_2) was added to the mixture. This increase implies that nanoparticles had a satisfactory effect of providing a density of coating, and to eliminate pores and micro-cracks, enhancing the protective barrier properties and the corrosion resistance efficiency, especially nano-silicon oxide, which showed the most effective performance of all types of models studied. At 298 K, the PHO/SiO2 nanocomposite exhibited higher Rp than the PHO/Al_2O_3 nanocomposite, with a Rp State clearly: SiO_2 gives higher Rp, whereas Al_2O_3 gives slightly higher PE% at 298 K, due to having the ability of nanoparticles to fill submicron-sized pores and defects within the PHO matrix and forming a denser and tighter barrier layer that inhibits corrosion of the metal

surface by the influx of corrosive chloride ions. The findings of this study align with the findings of previous investigations into the performance of nanocomposite coatings that were produced using silica-based fillers. Several studies have demonstrated improved corrosion resistance and barrier properties of nanocomposite coatings, which can be attributed to the homogenous distribution of nano-sized particles in the coating matrix [21].

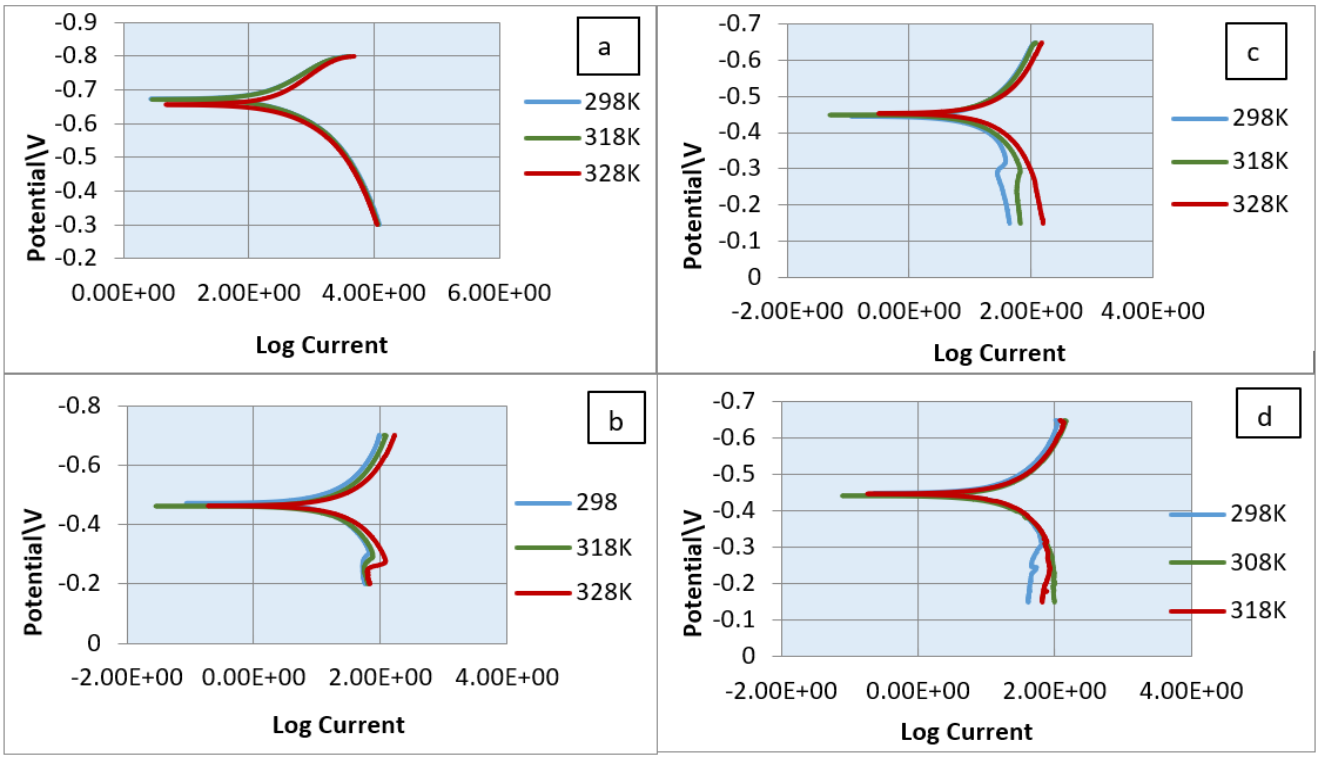

Figure 6. The polarization diagrams of (a) uncoated LCS, (b) PHO-coated LCS, (c) PHO-Al_2O_3 nanocomposite, and (d) PHO-SiO_2 nanocomposite

Note: LCS = low carbon steel; PHO = Poly(Z)-4-((4-hydroxyphenyl) amino)-4-oxobut-2-enoic acid.

Table 2. The properties of corrosion in the case of the LCS coated and uncoated with PHO at different temperatures in the presence of a saline solution (3.5% NaCl) with and without nanomaterials

Sample	T(K)	-E_{corr} (mV)	I_{corr} (mA/cm^2)	βc (mV/dec)	βa (mV/dec)	PL (mm/y)	R_p (Ω/cm^2)	PE%
Uncoated LCS	298	672	0.29000	107	81	1.423	145.5	
	308	674	0.30300	108	87	1.487	138.1	
	318	656	0.39830	128	96	1.955	119.7	
LCS\PHO	298	469	0.03593	259	260	0.176	2142	82.61
	308	466	0.07750	449	483	0.380	2607	88.14
	318	461	0.08815	395	411	0.433	1986	77.86
LCS\PHO\Al_2O_3	298	444	0.03958	232	235	0.194	2563	86.35
	308	442	0.05007	234	268	0.246	2166	83.47
	318	450	0.05624	240	297	0.276	2946	85.87
LCS\PHO\SiO_2	298	444	0.04054	278	400	0.199	3517	86.02
	308	448	0.04953	292	375	0.243	2878	83.65
	318	452	0.06224	283	314	0.305	2076	84.37

Note: LCS = low carbon steel; PHO = Poly(Z)-4-((4-hydroxyphenyl) amino)-4-oxobut-2-enoic acid.

Researchers looked at the impact of raising the temperature from 298 K to 318 K on the protective films' durability. Across the board, they found that as the temperature rose, the Rp and PE% for each of the samples went down. This is usually attributed to two factors: one, that the corrosion process is happening faster because of increased temperatures; and two, that a portion of the protective layer is being removed from the surface of the metal either through corrosion or due to heat alone. However, even at elevated temperatures, the nanocomposite coated samples demonstrated high levels of corrosion protection. The authors noted that while SiO_2-based coatings outperformed all other coatings at lower temperatures, the PHO/Al_2O_3 nanocomposite performed the best at 318 K with a PE% of 85.87% compared to the SiO_2-based nanocomposite (84.37%) and neat PHO coatings (77.86%). The authors also noted that it appears as though the addition of Al_2O_3 nanoparticles to the PHO coating enhanced both the adhesion and chemical stability of the PHO matrix at elevated temperatures [22]. Overall, the present findings confirm that the incorporation of nanomaterials into polymer coatings is an effective strategy for corrosion protection, in agreement with recent studies reporting the superior anticorrosive performance of SiO_2-based nanocomposite coatings [21].

3.6 Kinetic and thermodynamic corrosion activation parameters

Temperature is one of the important factors influencing the corrosion behavior of LCS in 3.5 wt.% NaCl medium, whether the steel surface is protected by a coating or left uncoated. Therefore, electrochemical tests, particularly potentiodynamic polarization measurements, were performed within the temperature range of 298-318 K for bare LCS, PHO-coated LCS, and PHO/metal oxide nanocomposite-coated LCS. These measurements were carried out to investigate the temperature dependence of the corrosion process and to determine the corresponding activation energy. The obtained data are summarized in Table 3. The Arrhenius relationships, represented by Eqs. (3) and (4), were applied to describe the formation of the activated complex at the transition state and to calculate the activation parameters related to corrosion [23]. Using the corrosion rate values measured at various temperatures, plots of log C.R against 1/T were generated for the uncoated, PHO-coated, and PHO/metal oxide nanocomposite-coated LCS samples, as illustrated in Figure 7. Furthermore, transition-state plots of log (C.R/T) versus 1/T were used to evaluate the thermodynamic activation parameters, including ΔH^* and ΔS^*, as shown in Figure 8.

Table 3. The kinetic and thermodynamic activation characteristics for uncoated and PHO-coated LCS discs with and without nanometal oxides at different temperatures

System	E_a^* (kJ\mol)	ΔH^* (kJ\mol)	ΔS^* (J/mol.K)
Uncoated LCS	12.411	9.767	-222.846
LCS\PHO	18.124	15.669	-216.237
LCS\PHO\Al_2O_3 nanocomposite	16.945	14.623	-222.806
LCS\PHO\SiO_2 nanocomposite	13.974	14.623	-222.806

Note: LCS = low carbon steel; PHO = Poly(Z)-4-((4-hydroxyphenyl) amino)-4-oxobut-2-enoic acid.

$$log\ C.R = log\ A - \frac{E_a}{2.303RT} \quad (3)$$

$$log\ \frac{C.R}{T} = log\left(\frac{R}{Nh}\right) + \frac{\Delta S^*}{2.303R} - \frac{\Delta H^*}{2.303RT} \quad (4)$$

where, C.R = the corrosion rate that is equivalent to the I_{corr}, Ea = the apparent effective activation energy, R = the molar gas ($JK^{-1}mol^{-1}$) constant, A = the Arrhenius preexponential factor, and T = the absolute temperature (K), N = Avogadro's number, h = Planck constant.

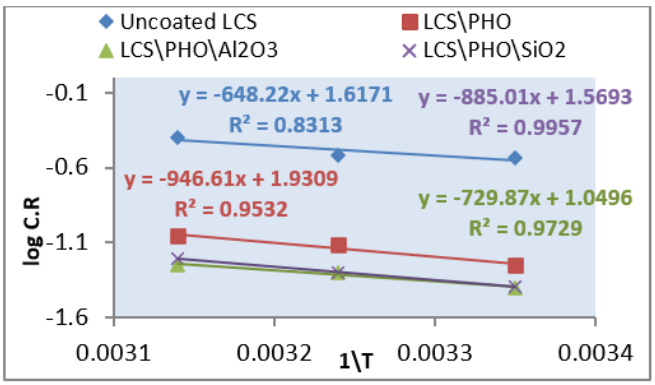

Figure 7. The relationship between log C.R and 1 T of uncoated LCS and LCS coated with PHO and PHO/metal oxide nanocomposites in 3.5% NaCl solution
Note: LCS = low carbon steel.

Results indicated that nanocomposites made using both PHO and PHO metal oxides covering LCS discs had greater values for thermodynamic activation parameters (Ea and H) as compared with uncoated LCS discs, indicating an increase in the energy barrier associated with these reactions. The coated and uncoated LCS entropy of activation (ΔS‡) values are both negative and change from negative to lower negative, meaning that the rate-limiting step associated with the formation of the activated complex from reactants was produced through the process of association rather than dissociation. There was also found to be less disorganization during the reaction between the reactants and the active complex [24].

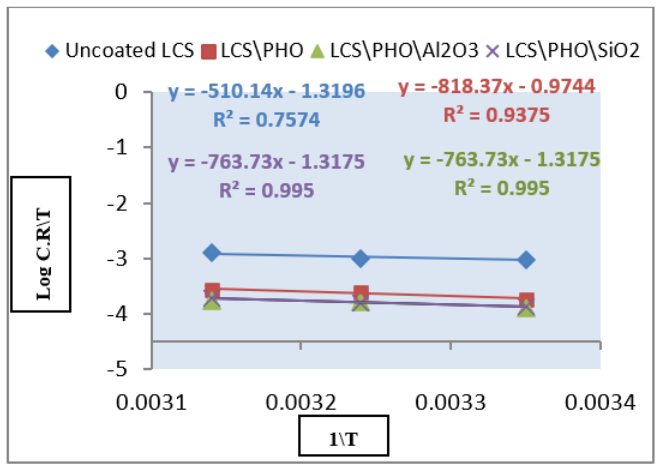

Figure 8. Log (C.R/T)–1/T plots for bare and coated LCS in 3.5 wt.% NaCl

3.7 Electrochemical Impedance Spectroscopy

Electrochemical impedance spectroscopy (EIS) was employed to investigate the electrochemical response of the corroding metal surface when subjected to a low-amplitude alternating potential over a range of frequencies. The impedance results were interpreted using Nyquist diagrams, in which the imaginary component of impedance (Z) is plotted as a function of the real component (Z). In addition, Bode representations were used to describe the frequency-dependent changes in the phase angle (o) and the impedance modulus (Z). From the Nyquist response, important corrosion-related parameters, such as impedance, capacitance, and Rp, can be determined. Moreover, the coating capacitance (C) of the polymer film and the uncompensated solution resistance (Rs) between the working and reference electrodes were estimated using the following equations [25, 26]:

$$C_C = \varepsilon\varepsilon^0 \frac{A}{d} \quad (5)$$

where, $\mathcal{E}^0$ is the dielectric constant in vacuum (8.85 × 10-12 A/cm), E is the dielectric constant of the polymer, d is the film thickness, and A is the area covered by the alloy.

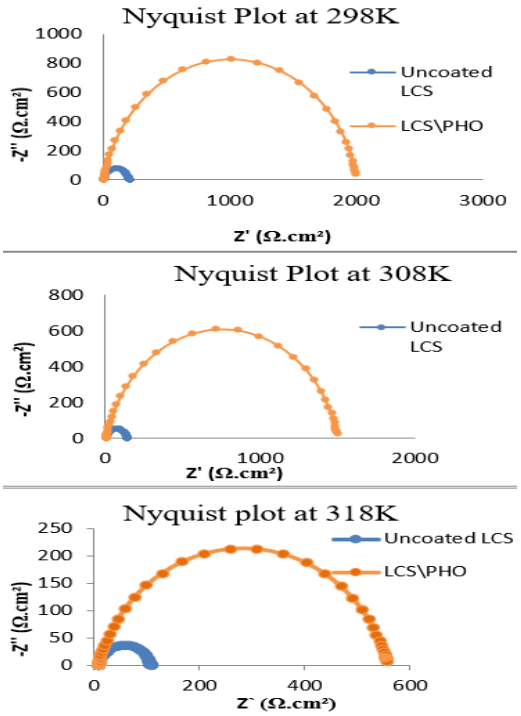

Figure 9. Nyquist plots of PHO coated and uncoated LCS at different temperatures in a 3.5% NaCl solution

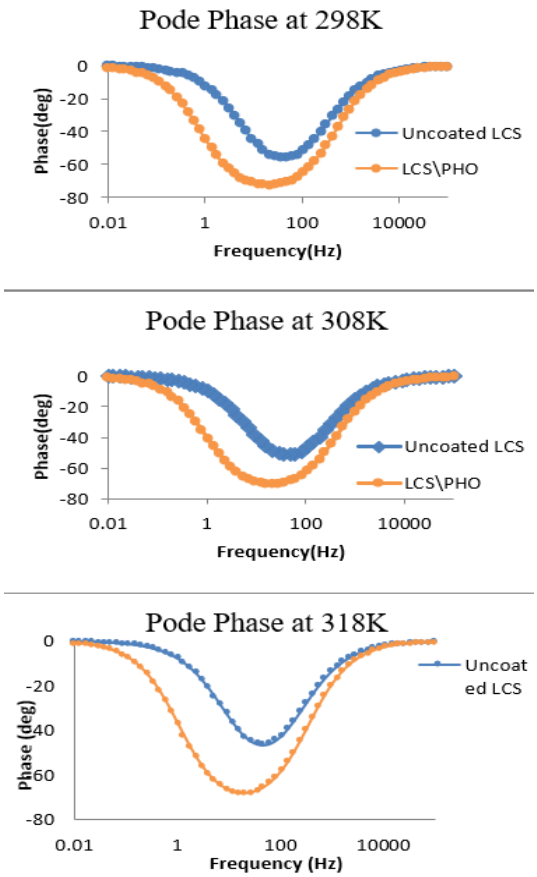

Figure 10. The PHO coated and uncoated LCS at different temperatures in a 3.5% solution of NaCl

Note: PHO = Poly(Z)-4-((4-hydroxyphenyl) amino)-4-oxobut-2-enoic acid; LCS = low carbon steel.

Figures 9-10 depict the experimental data of EIS of the LCS in the 3.5% NaCl solution under the investigation of uncoated and coated with PHO at three temperatures (298, 308, and 318 K) using the Nyquist plots and the Bode plots.

The results of EIS spectrum and the corresponding impedance parameters indicate that PHO coating hold significant corrosion resistance toward LCS discs in 3.5% NaCl solution via impeding the permeation of corrosive ions and water to a metal interface, does have a good physical barrier properties; The effectiveness of this protective layer is clearly highlighted by the very large increase in Rp for the coated system (LCS\PHO) compared to uncoated steel, with Rp values reaching upwards of 2000 Ω. cm^2 at 298 K, however these values are usually decrease with the increase in temperature since the thermal acceleration of the corrosion process.

In addition, the Bode plot analysis further confirms that the characteristic of coating performance is reflected in stable Rs and certain capacitive behavior (CPE), which validates that the polymer film can enhance barrier performances effectively by providing strong prevention of electrochemical reactions at the coating/metal interface [27]. They had the same equivalent circuit, as shown in Figure 11.

The analogous circuit yielded the following electrochemical parameters [28]:

Resistant electrolyte (Rs).

Rct = charge transfer resistance or Rp.

Constant phase element magnitude (CPE-Q).

CPE-n = phase shift or empirical exponent.

These parameter values are listed in Table 4.

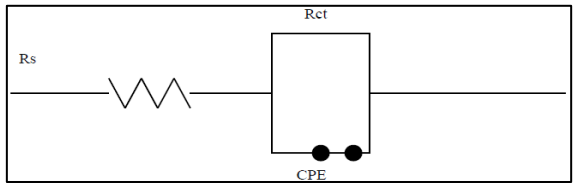

Figure 11. The analogous circuit for the coated and uncoated LCS

Note: LCS = low carbon steel.

Table 4. The electrochemical properties of an equivalent circuit of the PHO polymer-coated and untreated LCS discs

System	T (K)	RP (Ω.cm²)	Rs (Ω.cm²)	CPEQ (Ω.cm²)	CPE-n (Ω.cm²)
Uncoated LCS	298	200	7	0.00025	0.84
	308	140	7.5	0.0003	0.83
	318	100	8	0.00035	0.82
LCS\PHO	298	2000	7	0.00012	0.88
	308	1500	7.5	0.00014	0.87
	318	1100	8	0.00017	0.86

Note: PHO = Poly(Z)-4-((4-hydroxyphenyl) amino)-4-oxobut-2-enoic acid; LCS = low carbon steel.

4. CONCLUSIONS

The electropolymerization of HO monomer to form PHO and PHO/nanocomposite coatings on LCS was carried out in an aqueous solution (3.5% NaCl) through a DC power supply method. Potentiodynamic polarization on a solution of 3.5% NaCl was used to assess the corrosion inhibition efficiency of the polymer nano composite covering. The values of E_{corr} and the I_{corr} obtained from electrochemical

measurements/potentiodynamic polarization were governed by temperature. In the presence of nanomaterials, polymer sheets covered on LCS decreased the density of I_{corr}. The noble shift in E_{corr} suggests that the polymer layer contributes to anodic protection of polymer coated LCS with and without nanomaterials, compared to the uncoated LCS results in a Tafel plot shows that the polymer layer acts as anodic protection. The corrosion resistance for polymer nano composite coating is relatively high since the results show that it has better performance than bare LCS in terms of both corrosion inhibition efficiency and protection efficiency (PE%). In addition, because of the high degree of anti-corrosion properties, reliability, and simplicity of preparation of nano composite materials, they can further extend the range of anti-corrosion applications. The AFM study discusses details on this LCS, which was protected as a surface layer of protective coatings covered over the metal with greater barrier characteristics. The Rp of PHO-coated LCS was also determined at various temperatures to compare with that of uncoated LCS, and it was seen that Rp calculated from the measurement values was higher than that of uncoated LCS.

REFERENCES

[1] Yuan, X., Dragoe, D., Beaunier, P., et al. (2020). Polypyrrole nanostructures modified with mono- and bimetallic nanoparticles for photocatalytic H_2 generation. Journal of Materials Chemistry A, 8(1): 268-277. https://doi.org/10.1039/C9TA11088G

[2] Tkach, V.V., Kushnir, M.V., de Oliveira, S.C., et al. (2020). Theoretical aspects of the electropolymerization of some hydroquinonic derivatives. Biointerface Research in Applied Chemistry, 11(1): 7994-8000. https://doi.org/10.33263/BRIAC111.79948000

[3] Vázquez-Noriega, O.E., Guzmán, J., Gallardo-Rivas, N.V., et al. (2015). Polypyrrole films deposited on carbon-steel CS-1018 and its interaction with Mexican crude oil. International Journal of Electrochemical Science, 10(8): 6378-6391. https://doi.org/10.1016/S1452-3981(23)06726-3

[4] Ramezanzadeh, B., Niroumandrad, S., Ahmadi, A., Mahdavian, M., Moghadam, M.H.M. (2016). Enhancement of barrier and corrosion protection performance of an epoxy coating through wet transfer of amino functionalized graphene oxide. Corrosion Science, 103: 283-304. https://doi.org/10.1016/j.corsci.2015.11.033

[5] Palimi, M.J., Rostami, M., Mahdavian, M., Ramezanzadeh, B. (2015). A study on the corrosion inhibition properties of silane-modified Fe_2O_3 nanoparticle on mild steel and its effect on the anticorrosion properties of the polyurethane coating. Journal of Coatings Technology and Research, 12(2): 277-292. https://doi.org/10.1007/s11998-014-9631-6

[6] Mathai, S., Shaji, P.S. (2022). Polymer-based nanocomposite coating methods: A review. Journal of Scientific Research, 14(3): 973-1002. https://doi.org/10.3329/jsr.v14i3.58338

[7] Alqudsi, A.M., Saleh, K.A. (2023). Electrochemical polymerization of eugenol and corrosion protection studies of stainless steel 304L alloy. Journal of Medicinal and Chemical Sciences, 6(8): 1818-1829. https://doi.org/10.26655/JMCHEMSCI.2023.8.10

[8] Huang, T.C., Su, Y.A., Yeh, T.C., et al. (2011). Advanced anticorrosive coatings prepared from electroactive epoxy-SiO_2 hybrid nanocomposite materials. Electrochimica Acta, 56(17): 6142-6149. https://doi.org/10.1016/j.electacta.2011.04.053

[9] Yeganeh, M., Keyvani, A. (2016). The effect of mesoporous silica nanocontainers incorporation on the corrosion behavior of scratched polymer coatings. Progress in Organic Coatings, 90: 296-303. https://doi.org/10.1016/j.porgcoat.2015.11.006

[10] Wang, K., Ogier, P., Tjiu, C.W., He, C.B. (2006). Morphology and mechanical properties of epoxy/alumina nanocomposites. Key Engineering Materials, 312: 233-236. https://doi.org/10.4028/www.scientific.net/KEM.312.233

[11] Balaraju, J.N., Kalavati, Rajam, K.S. (2006). Influence of particle size on the microstructure, hardness and corrosion resistance of electroless Ni-P-Al_2O_3 composite coatings. Surface and Coatings Technology, 200(12-13): 3933-3941. https://doi.org/10.1016/j.surfcoat.2005.03.007

[12] Tallman, D.E., Levine, K.L., Siripirom, C., Gelling, V.G., Bierwagen, G.P., Croll, S.G. (2008). Nanocomposite of polypyrrole and alumina nanoparticles as a coating filler for the corrosion protection of aluminium alloy 2024-T3. Applied Surface Science, 254(17): 5452-5459. https://doi.org/10.1016/j.apsusc.2008.02.099

[13] Alqudsi, A.M., Saleh, K.A. (2024). Conducting polyanethole /metals oxides nanocomposites for corrosion protection and bioactivity. Baghdad Science Journal, 21(4): 1243. https://doi.org/10.21123/bsj.2023.8458

[14] Hussain, Z.A., Saleh, K.A. (2024). Corrosion protection performance of PACC and PACC-metal oxides nanocomposites electropolymerized coating of low carbon steel. Iraqi Journal of Physics, 22(2): 90-103. https://doi.org/10.30723/ijp.v22i2.1213

[15] Pickup, P.G., Osteryoung, R.A. (1984). Electrochemical polymerization of pyrrole and electrochemistry of polypyrrole films in ambient temperature molten salts. Journal of the American Chemical Society, 106(8): 2294-2299. https://doi.org/10.1021/ja00320a014

[16] Sadiq, S., Amaal, A.T., Entesar, O. (2020). Synthesis, characterization and investigation of new polymer contain heterocyclic derivatives as corrosion inhibitor for Stainless steel in acidic medium. European Journal of Molecular & Clinical Medicine, 7(2): 2020. https://doi.org/10.52711/0974-360X.2021.00644

[17] Wu, Y., Luo, Z., Wang, Y., Xu, C., Li, Y. (2025). Chitosan-grafted graphene oxide-reinforced bio-based waterborne epoxy nanocomposites for antibacterial and corrosion resistance in tropical marine environments: A mini-review. Polymers, 17(21): 2964. https://doi.org/10.3390/polym17212964

[18] Hussain, Z.A., Saleh, K.A. (2025). Electrochemical study of inhibition for low carbon steel corrosion in the saline medium through a novel polymer-metal oxides nanocomposite. Iraqi Journal of Science, 66(4): 1463-1477. https://doi.org/10.24996/ijs.2025.66.4.6

[19] Alqudsi, A.M., Saleh, K.A. (2024). Effect of graphene and Fe3O4 on the protection efficiency of polyeugenol conducted coating for stainless steel 316L in NaCl

solution. Baghdad Science Journal, 21(11): 3428-3437. https://doi.org/10.21123/bsj.2024.8876
[20] Amin, I., Batyrev, E., de Vooys, A., van der Weijde, H., Shiju, N.R. (2022). Covalent polymer functionalization of graphene/graphene oxide and its application as anticorrosion materials. 2D Materials, 9(3), 032002. https://doi.org/10.1088/2053-1583/ac54ee
[21] Khazaal, K.H., Alwash, O.A., Karafe, A.M. (2025). Environmentally sustainable alkyd-based SiO_2–CuO nanocoatings for industrial corrosion protection: Synergistic, structural, and electrochemical evaluation. Annales de Chimie - Science des Matériaux, 49(2): 163-175. https://doi.org/10.18280/acsm.490207
[22] Khudhair, N.A., Al-Sammarraie, A.M.A. (2019). Enhancing of corrosion protection of steel rebar in concrete using TiO_2 nanoparticles as additive. Iraqi Journal of Science, 60(9): 1898-1903. https://doi.org/10.24996/ijs.2019.60.9.2
[23] Deyab, M.A., Eddahaoui, K., Essehli, R., et al. (2016). Influence of newly synthesized titanium phosphates on the corrosion protection properties of alkyd coating. Journal of Molecular Liquids, 216: 699-703. https://doi.org/10.1016/j.molliq.2016.01.092
[24] Bazaka, K., Jacob, M.V., Crawford, R.J., Ivanova, E.P. (2012). Efficient surface modification of biomaterial to prevent biofilm formation and the attachment of microorganisms. Applied Microbiology and Biotechnology, 95(2): 299-311. https://doi.org/10.1007/s00253-012-4144-7
[25] Policastro, S.A., Anderson, R.M., Hangarter, C.M., Arcari, A., Iezzi, E.B. (2023). Incorporating physics-based models into equivalent circuit analysis of EIS data from organic coatings. Coatings, 13(7): 1285. https://doi.org/10.3390/coatings13071285
[26] Končan Volmajer, N., Steinbücher, M., Berce, P., Venturini, P., Gaberšček, M. (2019). Electrochemical impedance spectroscopy study of waterborne epoxy coating film formation. Coatings, 9(4): 254. https://doi.org/10.3390/coatings9040254
[27] Gong, J.Y., Wei, H., Hao, P., et al. (2024). Study on the influence of metal substrates on protective performance of the coating by EIS. Materials, 17(2): 378. https://doi.org/10.3390/ma17020378
[28] Raheem, K., Cassidy, J., Ryan, B., Betts, A. (2024). Monitoring the curing, degradation and moisture ingress into alkyl 2-cyanoacrylate adhesives using electrochemical impedance spectroscopy. Journal of Solid State Electrochemistry, 28(11): 4029-4040. https://doi.org/10.1007/s10008-024-06003-4

NOMENCLATURE

AFM	Atomic force microscopy
EIS	Electrochemical impedance spectroscopy
FTIR	Fourier transform infrared spectroscopy
H_2SO_4	Sulfuric acid
HO	(Z)-4-((4-hydroxyphenyl) amino)-4-oxobut-2-enoic acid
LCS	Low carbon steel
NaCl	Sodium chloride
PHO	Poly[(Z)-4-((4-hydroxyphenyl) amino)-4-oxobut-2-enoic acid]
SCE	Saturated calomel electrode
SiO_2	Silicon dioxide
Al_2O_3	Aluminum oxide

Latin symbols

A	Arrhenius factor, unit depends on the Arrhenius equation used
B_a	Anodic Tafel slope, V dec^{-1}
B_c	Cathodic Tafel slope, V dec^{-1}
C_c	Capacitance of the polymer film, F cm^{-2}
CPE	Specific capacitive behavior
CPE-n	Empirical exponent or phase shift, dimensionless
CPE-Q	Constant phase element magnitude, unit depends on the fitted EIS model
E_a*	Activation energy, kJ mol^{-1}
E_{corr}	Corrosion potential, V
I_{corr}	Corrosion current density, A cm^{-2}
PE	Protection efficacy, dimensionless
PL	Penetration loss, mm y^{-1}
R_{ct}	Charge transfer resistance, ohm cm^2
R_p	Polarization resistance, ohm cm^2
R_s	Solution resistance, ohm
S_a	Average roughness, nm
S_q	Root mean square roughness, nm
T	Absolute temperature, K

Greek symbols

ΔH*	Activation enthalpy, kJ mol^{-1}
ΔS*	Activation entropy, J mol^{-1} K^{-1}
η	Protection efficacy, dimensionless
Θ	Phase angle, degree

Subscripts

p	nanoparticle
f	fluid (pure water)
nf	nanofluid
a	Anodic
c	Cathodic